

USE OF MODAL ACOUSTIC EMISSION TO MONITOR DAMAGE PROGRESSION IN CARBON FIBER/EPOXY AND IMPLICATIONS FOR COMPOSITE STRUCTURES

J. M. Waller¹, C. T. Nichols², D. J. Wentzel³ and R. L. Saulsberry⁴

¹Materials Scientist, NASA Johnson Space Center White Sands Test Facility, Laboratories Department, MS 200LD, Las Cruces, New Mexico 88011.

²USRP Intern, Dept. of Mechanical and Aerospace Engineering, New Mexico State University, Las Cruces, New Mexico 88003.

³USRP Intern, Dept. of Physics, Miami University, Oxford, Ohio 45056

⁴Project Manager, NASA Johnson Space Center White Sands Test Facility, Laboratories Department, MS 200LD, Las Cruces, New Mexico 88011.

ABSTRACT. Broad-band modal acoustic emission (AE) data was used to characterize micromechanical damage progression in uniaxial IM7 and T1000 carbon fiber-epoxy tows and an IM7 composite overwrapped pressure vessel (COPV) subjected to an intermittent load hold tensile stress profile known to activate the Felicity ratio (*FR*). Damage progression was followed by inspecting the Fast Fourier Transforms (FFTs) associated with acoustic emission events. FFT analysis revealed the occurrence of cooperative micromechanical damage events in a frequency range between 100 kHz and 1 MHz. Evidence was found for the existence of a universal damage parameter, referred to here as the critical Felicity ratio, or Felicity ratio at rupture (*FR**), which had a value close to 0.96 for the tows and the COPV tested. The implications of using *FR** to predict failure in carbon/epoxy composite materials and related composite components such as COPVs are discussed. Trends in the FFT data are also discussed; namely, the difference between the low and high energy events, the difference between early and late-life events, comparison of IM7 and T1000 damage progression, and lastly, the similarity of events occurring at the onset of significant acoustic emission used to calculate the *FR*.

Keywords: modal acoustic emission; Felicity ratio; fast Fourier transform, COPV

PACS: 43.40.Le Techniques for nondestructive evaluation and monitoring, acoustic emission

INTRODUCTION

Composite Overwrapped Pressure Vessels (COPVs) (Figure 1) are widely used in launch vehicles and satellites, where the strong drive to reduce weight has pushed COPV designers to adopt high performance, high specific strength composite materials with a relatively high volume fraction ($v_f \approx 0.6$ to 0.7) of fiber. To date, the composite materials used in COPV designs have typically consisted of aramid or carbon fiber embedded in a thermoset matrix such as epoxy. The role of the matrix is to transfer pressurization load to the fiber, while the role of the fiber is to withstand the load over time under the environmental exposure conditions encountered in service. Pressures of 35 to 70 MPa (5000 to 10,000 psi) are common for COPVs. This has necessitated the use of high load bearing composite overwraps wound around a thin-walled metal liner.

NASA has been faced with recertification and life extension issues for both epoxy-impregnated Kevlar[®] 49 (K/Ep) and epoxy-impregnated carbon (C/Ep) COPVs used in various systems on the Space Shuttle and International Space Station, respectively. Each COPV has varying criticality, usage histories, damage and repair histories, time at pressure,



FIGURE 1. NASA carbon-epoxy fleet leader composite overwrapped pressure vessels

and number of pressure cycles. COPVs are of particular concern due to the insidious and catastrophic “burst-before-leak” (BBL) failure mode caused by stress rupture (SR) of the composite overwrap. SR life has been defined by the American Institute for Aeronautics and Astronautics (AIAA) Aerospace Pressure Vessels Standards Working Group as “the minimum time during which the composite maintains structural integrity considering the combined effects of stress level(s), time at stress level(s), and associated environment” [1]. SR has none of the features of predictability associated with metal pressure vessels, such as crack geometry, growth rate and size, or features that lend themselves to the use of nondestructive evaluation (NDE) methods. In essence, the variability or “surprise factor” associated with SR in COPVs cannot be eliminated. For these reasons, NASA has devoted much effort to develop NDE methods that can be used during post-manufacture qualification, in-service inspection, and in situ structural health monitoring. One of the more promising NDE techniques for detecting and monitoring, in real-time, the strain energy release and corresponding stress-wave propagation produced by actively growing flaws and defects in composite materials is acoustic emission (AE) [2, 3, 4, 5, 6, 7, 8, 9]. It is hoped that the procedures described in this paper lay the groundwork for establishing critical thresholds for accumulated damage in composite structures such as COPVs so that precautionary or preemptive engineering steps can be implemented to minimize or obviate the risk of catastrophic failure.

EXPERIMENTAL

Tensile Testing

Programmed intermittent load hold (ILH) stress schedules were applied using an Instron[®] 5569 Series Electromechanical Test Instrument equipped with a 50 kN (11,200 lb_f) capacity load cell. Other features included self-tightening 25 × 51 mm (1 × 2 in.) wedge action mechanical grips, and Bluehill[®] data acquisition software (version 1.8.289). To minimize excessive AE during loading and unloading ramps, a 20 N/min (4.5 lb_f/min) loading/unloading rate was used, consistent with ASTM E 1118 [10] recommendations. To prevent saturation of the Bluehill[®] data acquisition buffer, a 1 to 2 s⁻¹ data acquisition rate

was used, depending on the duration of test (tests generally took 7 to 16 h to complete). Tensile test data acquisition was synchronized with AE data acquisition (see next section) to facilitate monitoring of progressive damage accumulation as a function of applied stress.

Composite strand specimens and the COPV test article were subjected to similar ILH stress schedules (Table 1 and Figure 2). The stress schedule used was based on the pressure tank examination procedure described in ASTM E 1067 [11] and similarly referred to as the manufacturer's qualification test in ASTM E 1118 [10]. The ILH method was chosen because it expedited determination of trends in the *FR*, allowing tests to be completed in one day or less.

TABLE 1. Description of Intermittent Load Hold (ILH) Stress Schedules

| composite strand ILH | COPV ILH |
|--|--|
| 1. Ramp: Load to 530 N (120 lb _f) | 1. Ramp: Pressurize to 13.8 MPa (2000 psig) |
| 2. Load Hold: 10-min | 2. Pressure Hold: 30-min |
| 3. Ramp: Unload 90 N (20 lb _f) | 3. Ramp: Depressurize 2.76 MPa (400 psig) |
| 4. Load Hold: 10-min | 4. Pressure Hold: 30-min |
| 5. Ramp: Load 220 N (50 lb _f) to next highest load | 5. Ramp: Pressurize 6.89 MPa (1000 psig) to next highest pressure |
| 6. Repeat Steps 2-5 until ultimate tensile strength reached | 6. Repeat Steps 2-5 until 46.9 MPa (6800 psig) or burst strength reached |

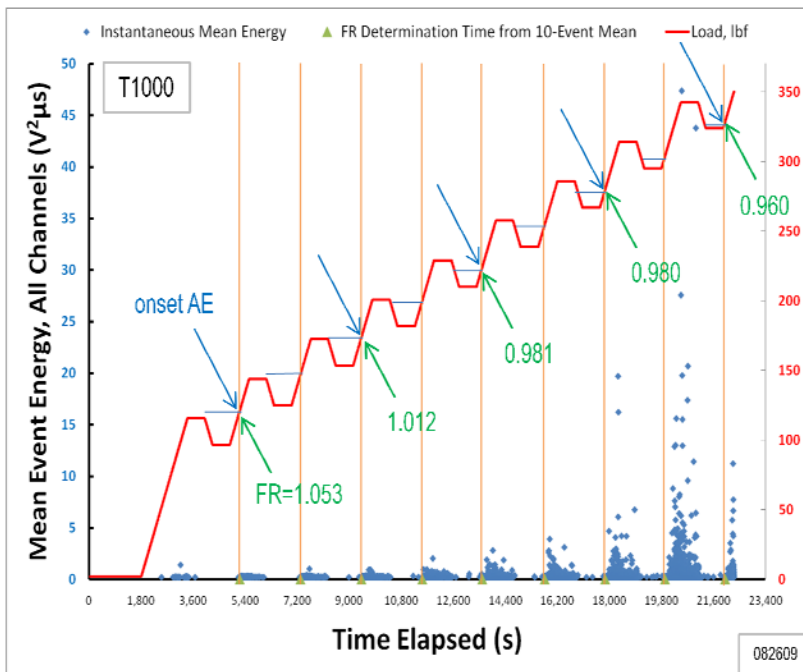


FIGURE 2. Representative intermittent load hold stress schedule used for T1000 carbon-epoxy composite strand showing decrease in onset AE relative to previous highest load, and Felicity ratio with time (right y-axis units are in lb_f)

Acoustic Emission

AE measurements were taken using a model FM-1 (Digital Wave Corp., Centennial, CO) signal conditioner equipped with 8-channel capability. Four or six channels were during strand tests or the COPV test, respectively. For composite strand tests, each channel

was connected to a DWC PA-0, 0 dB gain preamplifier, and then to a broadband, high fidelity B1080 piezoelectric sensor with a frequency range of 50 kHz to 1.5 MHz. For the COPV test, B1025 sensors with a frequency range of 100 kHz to 3.0 MHz were used, along with the available FM-1 parametric channel. The parametric channel allowed COPV pressure and AE data to be synchronized. Sensors were attached to the composite strand (same side) or COPV using a 10:1 Lord 202 acrylic adhesive:Lord 17 accelerant ratio. The adhesive was allowed to cure for 30 min. The AE system was supported with a lunchbox computer equipped with WaveExplorer™ software (versions 6.2 and 7.2). The software allowed arrival time, event energy, and event time to be acquired for all registered events. Sensor sensitivity was checked using pencil lead breaks performed midway between adjacent sensors, according to guidelines described in ASTM E 976 [12]. A default velocity of 4600 m s^{-1} for propagation of elastic stress waves in graphite was used in all IM7 and T1000 tests. Prior to initiating the ILH stress schedule (Table 1, Step 1), AE data was collected for 30 min on the unloaded strand/unpressurized COPV to determine background.

Details of AE data reduction and calculation of the Felicity ratio (FR) are given elsewhere [13, 14, 15]. Better procedures that consist of isolating the direct wave and removing reflections [16] were not used in this study, but will be discussed later at the end of the ‘FFT Analysis’ section. Fast Fourier transforms (FFTs) were obtained using the WaveExplorer™ software and using raw AE data. To expedite analysis, only events that occurred on the ILH up-ramps were analyzed. As a further simplification, only first arrival channel FFTs were analyzed. FFTs were exported to Microsoft Excel™ and the area under the frequency curve was calculated using a right Riemann sum and a step size equal to the default interval between frequencies (0.49 kHz).

Materials

Composite Strand: Unidirectional 3817 denier Torayca® T1000G ($v_f \approx 0.676$ to 0.707) and 3775 denier HexTow™ IM7 (5000) ($v_f \approx 0.670$ to 0.708) 12,000-filament composite strands had an ultimate tensile strength (UTS) of $6.81 \pm 0.37 \text{ GPa}$ ($988 \pm 53 \text{ ksi}$) and $3.96 \pm 0.31 \text{ GPa}$ ($575 \pm 45 \text{ lb}_f$), respectively. Each specimen had ribbon-like geometry with irregular width and thickness. The load bearing cross-sectional area was calculated as $A = n\pi(D^2/4)$, where n was the number of filaments in the tow and D was the diameter of a single filament, or 0.236 mm^2 (365 mil^2) and 0.255 mm^2 (395 mil^2) for T1000 and IM7, respectively. A gage length of 25 cm (10 in.) was used in each test. Each specimen had cardboard end tabs with an $l \times w$ of $25 \text{ mm} \times 51 \text{ mm}$ ($1 \text{ in.} \times 2 \text{ in.}$). Tow ends were secured to the cardboard with a 3.5 gr. (0.12 oz) bead of 1:1 Hardman® Extra-Fast Setting Epoxy (Ellsworth Adhesives, Germantown, WI) which cured for at least 24 h prior to testing. The cardboard end tabs were designed with two, stacked $25 \times 1 \times 1 \text{ mm}$ ($1 \times 0.079 \times 0.079 \text{ in.}$) cardboard spacers on the outside edge of each tab, thus increasing the amount of epoxy held within the tab (Figure 3, left). These spacers account for the 3.0 mm (0.12 in.) thickness of the tab end dimensions. This change reduced the propensity of pullout at higher stresses, reduced grip noise (amount data filtered from raw AE data sets decreased from > 30 percent to < 10 percent), and reduced the stress on the specimen caused by the grips (fewer grip failures were observed). C/Ep strands were aligned perpendicular to the 25-mm tab edge to insure tensile loading would not cause shear or torsional stresses within

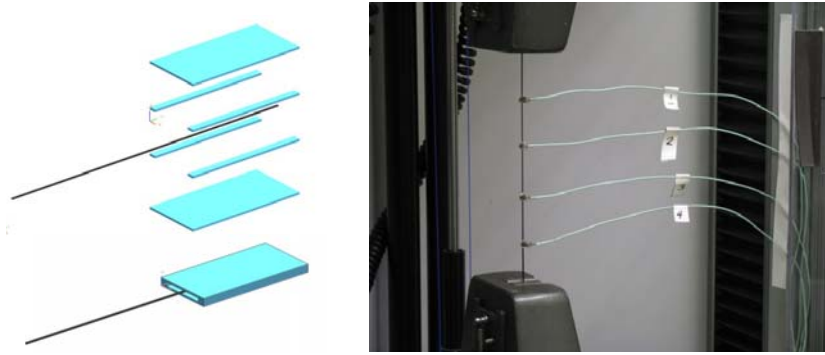


FIGURE 3. Cardboard end tabs before and after assembly (left, adhesive not shown), and a 25-cm gauge length 12k carbon-epoxy tow specimen mounted in grips showing four B1080 AE sensors (right, end tabs hidden in grips).

the specimen. The specimens were mounted vertically with four AE sensors positioned approximately 4 cm (1.6 in.) from each other (Figure 3, right). Composite strands were fabricated by wrapping prepreg tape over a steel mandrel subjected to the same cure cycle as the COPV (below); however, the strands were not vacuum bagged during curing.

COPV: COPV fabrication (S/N 070908-02) was conducted at HyPerComp Eng. Inc. (Westlake, CA) and consisted of wrapping a cylindrically shaped aluminum liner (Samtech International, Inc.) with TCR™ prepreg tape (ATK Space Systems, Ogden, UT) made from 3775 denier IM7-W-12K fiber impregnated with UF3323-102 resin. The COPV had a nominal outer diameter (OD) of 16.0 cm (6.3 in.), length of 50.0 cm (19.8 in.) and a nominal wall thickness of 2.0 mm (0.080 in.). Wrap pattern 3H/15C was used to overlay the liner. The helical angles, indicated by “H” representing 2 plies (both a + and -) of helical wraps, were oriented at 13.8° and 17.1° respectively with an average angle of 14.9° relative to the vessel’s axial direction. The cirque or “hoop” wrap was one ply. Hydroburst tests of two vessels of identical design to the one tested here gave a burst pressure of 51.91 ± 1.01 MPa (7529 ± 147 psi). The COPV was instrumented with six AE sensors as described in Table 2. The corresponding sensor spacing was determined to be adequate for picking up higher frequency AE attributable to fiber breakage. During the COPV ILH profile (Table 1), the COPV was pressurized during the ILH up-ramps at 0.07-0.08 *LR*/min (~10 psi/sec) (*LR* = load ratio = instantaneous load/pressure divided by the ultimate load/pressure). A low initial pressurization to $LR \approx 0.27$ was also used so that *FR* data could be collected throughout the autofrettage and operational pressurization ranges. The COPV ILH test experienced little background noise and low electromagnetic interference.

TABLE 2. Acoustic Emission Sensor Map Used for Intermittent Load Hold Composite Overwrapped Pressure Vessel Test

| AE Sensors (B1025) | |
|---------------------------|--|
| Sensor No. | Location |
| 1 | 0°, 4.5 in. from edge of top boss |
| 2 | 180°, 4.5 in. from edge of top boss |
| 3 | 270°, Equator |
| 4 | 90°, Equator |
| 5 | 180°, 4.5 in. from edge of bottom boss |
| 6 | 0°, 4.5 in. from edge of bottom boss |

RESULTS AND DISCUSSION

Felicity Ratio Analysis

One of the most significant findings in the previous work on K/Ep tow [13] and carbon-epoxy tow [14, 15] was the observation of highly linear decreases in the FR with increasing stress during ILH testing. Also, while acceptable linearity ($R^2 > 0.9$) was obtained on K/Ep tow [13] by using first significant AE event to determine the onset of significant AE, acceptable linearity could only be obtained on C/Ep tow using the first 5, 10, 15, or 20 significant ‘onset’ AE events.

All IM7 and most T1000 (4 of 6) composite strand specimens that gave acceptable breaks in the gage region, failed explosively (‘X’ designation, Table 3, last column). Taking $FR=1$ as the threshold for significant accumulated damage, a mean load threshold of 743 N (167 lbf) was obtained for IM7, and 939 N (211 lbf) for T1000 (Table 3, column 2). Another parameter, denoted here as FR^* , or critical Felicity ratio (Table 3, next-to-last column), was developed to estimate the FR at which failure would occur using the linear least squares fit to extrapolate the hypothetical FR value at failure. Both IM7 and T1000 gave $FR^* \approx 0.96$, with an observed scatter between 1.2 and 1.4 percent. The ultimate tensile strength gave much more scatter, varying between 5.3 and 7.9 percent, indicating that the FR is more independent of failure mode than the tensile strength, or in the case of a COPV, the burst pressure. These observations suggest that FR is a more reliable failure parameter than tensile or burst strength.

Examination of the relationship between the slope of the FR line and the damage tolerance of the material (Figure 4) is also instructive. IM7 and T1000 have similar damage tolerances, with T1000 being slightly more damage tolerant than IM7. K/Ep, although quieter than C/Ep during loading on the basis of the number of AE events that were detected [13], undergoes a steeper and more dramatic drop in FR upon loading, and therefore, may be thought to be less damage tolerant than C/Ep. This seem counterintuitive (fewer events = less damage tolerant) until it is realized that the AE events associated with K/Ep damage tended to be more energetic [13] than the events associated with C/Ep damage.

Application of Felicity Ratio to a COPV

IM7 COPV data (large crossed hexagonal symbols, Figure 4) were found to overlap and IM7 strand data (grey symbols, dashed lines, Figure 4) using FR s calculated the same

TABLE 3. Intermittent Load Hold Tensile Test Results for T1000 and IM7 12k Carbon-epoxy Strands¹

| Material & Spool # | F @ FR=1 (lb _f) | F _{max} (lb _f) | σ @ FR=1 (ksi) | σ _{max} (ksi) | FR* | Failure ² |
|--------------------|-----------------------------|-------------------------------------|----------------|------------------------|--------------|----------------------|
| IM7 #95 | 135 | 210 | 342 | 532 | 0.950 | XGB |
| IM7 #95 | 151 | 234 | 383 | 591 | 0.945 | XGM |
| IM7 #95 | 171 | 210 | 433 | 530 | 0.971 | XGM |
| IM7 #117 | 193 | 252 | 488 | 637 | 0.961 | XGM |
| IM7 #61 | 183 | 228 | 464 | 578 | 0.970 | XGM |
| Mean IM7 | 167 | 227 | 422 | 575 | 0.959 | |
| Std. Dev. | 24 | 18 | 60 | 45 | 0.012 | |
| T1000 #74 | 240 | 355 | 658 | 972 | 0.972 | XGT |
| T1000 #74 | 231 | 369 | 633 | 1010 | 0.953 | XGT |
| T1000 #74 | 226 | 362 | 618 | 992 | 0.977 | XGT |
| T1000 #155 | 181 | 379 | 497 | 1037 | 0.945 | SGM |
| T1000 #74 | 206 | 325 | 564 | 890 | 0.966 | LGM |
| T1000 #155 | 181 | 374 | 493 | 1024 | 0.950 | XGM |
| Mean T1000 | 211 | 361 | 577 | 988 | 0.961 | |
| Std. Dev. | 26 | 19 | 71 | 53 | 0.013 | |

¹ Abbreviations used: FR = Felicity ratio, FR* = Felicity ratio at rupture (extrapolated), F = force, σ = stress

² Failure abbreviations per ASTM D 3039, *Test Method for Determining Tensile Properties of Polymer Matrix Composite Materials*, American Society for Testing and Materials, West Conshohocken, PA (2007)

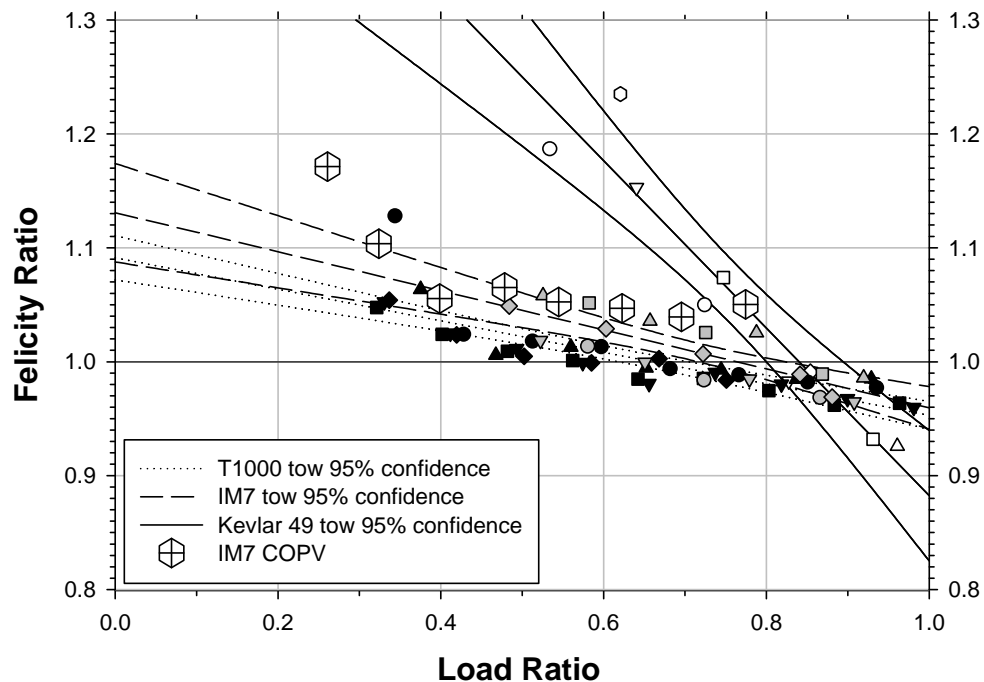


FIGURE 4 Least squares fits and 95 % confidence intervals for T1000 carbon-epoxy strand (black symbols, dotted lines), IM7 carbon-epoxy strand (grey symbols, dashed lines), Kevlar®-epoxy composite strand (white symbols, dashed lines), and an IM7 composite overwrapped pressure vessel (large crossed hexagonal symbols)

NOTE: Felicity ratios depicted here were determined using the first AE event for Kevlar®-epoxy strand, and the mean of the first 15 events for T1000 strand, IM7 strand, and the single IM7 COPV.

way (first 15 events averaged to determine the onset of significant AE). This overlap suggested that the IM7 COPV was trending towards failure in much the same way IM7 composite strands were (Table 3). To determine if this was true, the IM7 COPV was taken to burst in a subsequent ILH test that consisted of ramping to 34.5 MPa (5000 psig) and repeating Step 2-5 (Table 1, right column) until burst was reached.

Stitching the two COPV ILH data sets together initially proved difficult. However, acceptable congruence between the two data sets was obtained by using an in-house FR determination method. Predicting a COPV's burst pressure, P^* , has proven to be difficult as evidenced by the wide Weibull variability of C/Ep COPVs [17]. However, if FR dependence on LR is known for a group of vessels having the same design and materials-of-construction, FR^* may be used to predict P^* semi-empirically using the following expressions:

$$FR^* = (mP^* + b)[1 \pm (1 - R^2)^2] \quad (1)$$

$$P^* = \left(\frac{FR^* - b}{m} \right) [1 \pm (1 - R^2)^2] \quad (2)$$

where m is the FR versus LR slope, and b is the hypothetical zero load FR . In the IM7 COPV test conducted in this study, the FR^* was found to be 0.961 ± 0.018 using the in-house FR determination method alluded to above, and Eq. (1) ($m = -3.099 \times 10^{-5}$, and $b = 1.205$, $R^2 = 0.865$). Note that the COPV FR^* (0.961) is nearly identical to the strand FR^* (0.959) (see Table 3). Assuming that COPV FR^* s exhibit the same scatter as strand FR^* s (next-to-last column in Table 3), the FR method should be able to predict the burst pressure to within several percent. Application of Eq. (2) verifies this, giving a P^* of 54.3 ± 1.0 MPa (7870 ± 144 psi), which has a 1.8 percent margin of error. Fortuitously, the observed burst pressure was 54.25 MPa (7869 psi). This remarkable agreement definitively demonstrates the promise of the FR trend analysis to predict the burst pressure of COPVs. However, it must be noted that first COPV ILH data set, which involved taking the COPV to 46.9 MPa (6800 psi), or an LR of 0.86, would have led to a much more conservative prediction of $P^* = 51.98$ MPa (7540 psi), which interestingly, is almost in exact agreement with the measured burst pressure of 51.91 ± 1.01 MPa (7529 ± 147 psi) for IM7 COPVs of the same design (P^* based on $FR^* = 1.000$, $m = -2.281 \times 10^{-5}$, and $b = 1.172$, $R^2 = 0.900$). The observation of a higher FR^* of 1.000 (>0.961) at $LR = 0.87$ may also have been an strong indicator of a higher than expected burst strength, which is exactly what was observed. Additional work is needed to verify if such FR versus P trends consistently predict in-family or out-of-family behavior. Also, it is presently unknown if ILH tests conducted at lower LR s (~ 0.4 to 0.6) that coincide with operation pressures would lead to poorer predictions of P^* ; however, this concern may be moot since the anticipated approach to $FR^* \approx 0.96$ during late life, regardless of the LR , should be given more weight when evaluating the health of a COPV overwrap.

Waveform Analysis

In this study, the range of 90 to 190 kHz was attributed to matrix cracking, the range of 190 to 300 kHz to fiber pullout and debonding, while frequencies above 300 kHz were attributed to fiber breakage [4]. This microdamage assignment scheme allowed several characteristic waveforms to be identified during ILH testing of C/Ep strand, each

differentiated on the basis of AE event amplitude, duration and frequency. The first characteristic waveform exhibited low amplitude signals with lower frequencies and short durations (Figure 5). This waveform was attributed to matrix cracking. The second waveform observed tended to exhibit moderate amplitudes with high frequencies and short durations. This was attributed to fiber breakage (Figure 6). The final waveform observed tended to exhibit high amplitudes and a wide range of frequencies and long durations (Figure 7). This was attributed to concerted failure including all modes of micromechanical damage (as shown in Figures 5 and 6), plus fiber pullout and debonding, which did not appear as a discrete event. These conclusions were based on FFT analysis [4] and other related research [9]. The most frequently encountered waveform, especially during the ILH loading up-ramps, was determined to be concerted failure (Figure 7).

FFT Analysis

AE event energy as given by the maximum amplitude at first arrival channel varied significantly event to event. It was initially hypothesized that high energy events were attributable to fiber breakage, and therefore, should be characterized by FFTs with higher frequency peaks. To determine if this was true, the AE event FFTs with energies less than $2.0 \text{ V}^2\mu\text{s}$ (denoted ‘low energy’), were compared to event FFTs with energies greater than $2.0 \text{ V}^2\mu\text{s}$ (denoted ‘high energy’). The percent energy release was calculated by dividing energy released within a certain frequency range (units $\text{V}^2 \mu\text{sec} \times \text{sec}$) by the total energy released with all frequency ranges between 90 and 900 kHz. A random sampling of high and low energy events occurring during the ILH up-ramps (Step 5 in Table 1, left column) were used in this calculation.

Contrary to expectation, low energy events (Figure 8, left) were found to correspond to predominant fiber breakage. The percent energy release attributable to fiber breakage was also found to be independent of the *LR* (time is proportional to *LR* in Figure 8). The second most prominent damage mechanism was matrix cracking, and the third was fiber-matrix debonding and pull-out. This damage hierarchy was consistent for both IM7 and T1000 low energy events for all *LR*s.

The high energy events did not exhibit a consistent damage hierarchy (Figure 8, right), but instead exhibited a mixture of all micromechanical damage modes. In addition, it was observed that matrix cracking dominated the first ILH up-ramp. This is consistent with observations by various researchers [18, 19] who contend that the majority of damage in an unstressed composite is due to transverse matrix cracking, at least for quasi-isotropic composites subjected to biaxial stress. Such AE is primarily related to sources generated by the formation of the characteristic damage state (Step 1, Table 1), which is a consequence of the incompatibility of strains due to the large differences in the elastic modulus and strength of the fibers compared to the polymer matrix. In the case of uniaxial loading parallel to the fiber axis (this study), microdamage during the first loading attributable to transverse matrix cracking would be expected to be not as important, while microdamage attributable to fiber breakage caused by preexisting fiber flaws or fiber misalignment would be expected to be more important. Data will be presented below that provides evidence that this is exactly what occurs in uniaxial IM7 and T1000 composite strand specimens.

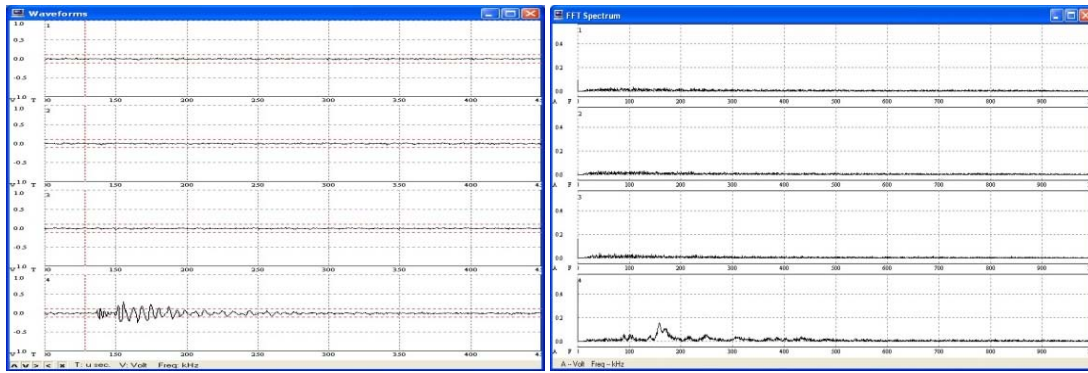


FIGURE 5 Carbon-epoxy 12k strand matrix cracking event amplitude vs. time waveform (left) and unfiltered amplitude vs. frequency fast Fourier transform (right)

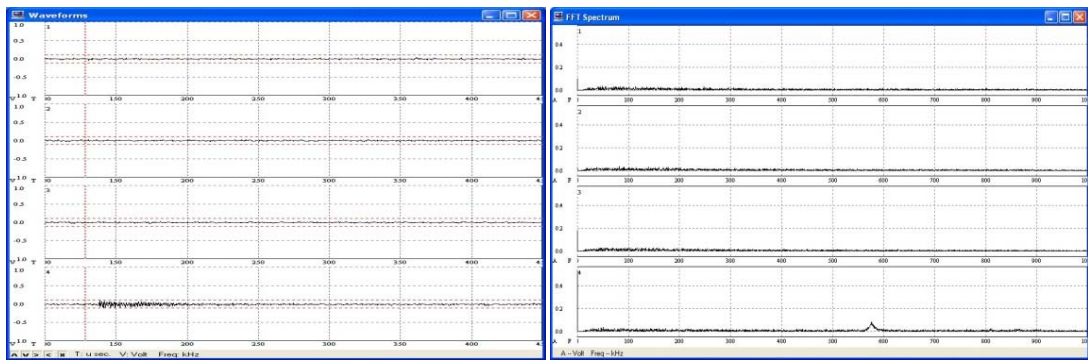


FIGURE 6 Carbon-epoxy 12k strand fiber breakage event amplitude vs. time waveform (left) and unfiltered amplitude vs. frequency fast Fourier transform (right)

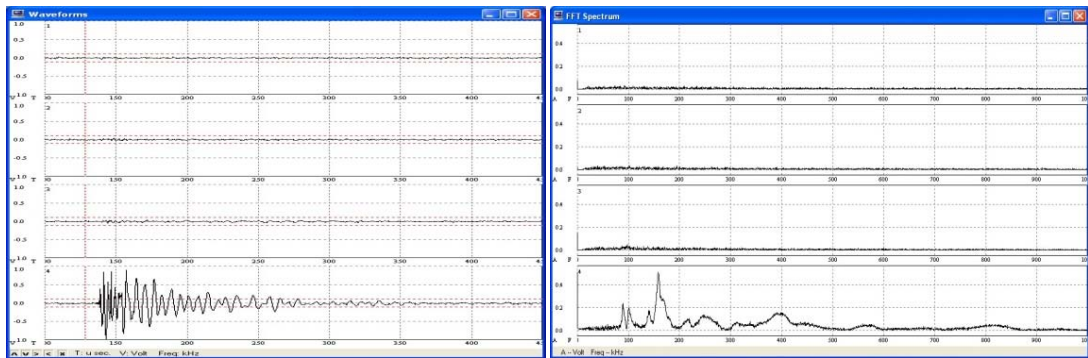


FIGURE 7 Carbon-epoxy cooperative matrix cracking, fiber-matrix debonding and pull-out, and fiber breakage event amplitude vs. time waveform (left) and unfiltered amplitude vs. frequency fast Fourier transform (right)

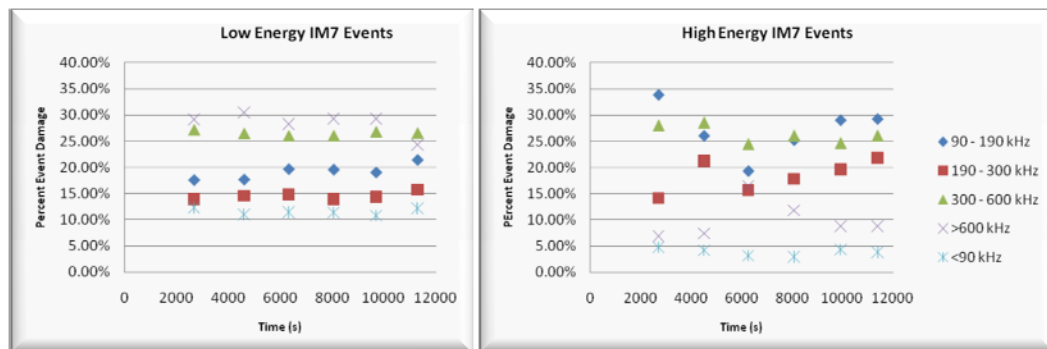


FIGURE 8 AE event low (left) and high energy release distribution for IM7 carbon-epoxy 12k strand

FFT frequency distribution of early and late life AE events for a representative IM7 strand specimen was then investigated (data not shown). More specifically, early life events occurring on the first ILH up-ramp (Step 1, Table 1) were compared to late life AE events occurring on the last up-ramp preceding to failure (at 1030 N (232 lb_f)). Early life events exhibited similar frequency distributions and the observed peaks were comparable in amplitude and width, while late life events exhibited a larger range of frequencies, with the observed peaks showing few similarities in peak amplitude and width. This shift from ordered frequency distribution to increasingly random frequency distribution suggests that the onset of significant accumulated damage is accompanied by increasing complex and cooperative damage mechanisms. Such complexity may arise from damage to both the epoxy matrix and carbon filaments, which would in turn would affect the propagation of AE signals, leading to an increased propagation velocity due to increased modulus during early life, and a decreased propagation velocity due to decreased modulus during late life.

FFT analysis was also performed on the *FR* events responsible for the onset of significant AE during the ILH up-ramps (i.e., AE associated with the creation of new flaw sites, or the growth of existing ones). Frequency distributions for these events were found to be invariant with respect to *LR* (Figure 9) and essentially the same for T1000 versus IM7 (data not shown). Also, fiber breakage (>300 kHz) was the most predominant failure for both IM7 and T1000. It was noticed that T1000 had slightly more low frequency damage associated with matrix cracking than IM7. It is hypothesized that this is due to the higher fiber strength of the T1000 versus IM7 filaments, thus localized stresses would be expected to cause more matrix damage compared to fiber damage at equivalent *LR*s. Also, ultrahigh (> 600 kHz) frequency events were more prominent in IM7 specimens (> 30 percent of total event damage) than in T1000 specimens (< 30 percent).

More strand and COPV specimens must be analyzed to verify that such differences are not caused by scatter or that the damage hierarchies presented above are not affected adversely by using raw instead of direct wave FFT data (with any reflections also removed). Recalculated FFT distributions for the IM7 COPV ILH test using only the direct wave (data not shown) show that fiber breakage dominates early and mid life, but is surpassed by matrix cracking in late life. This subtle shift may be due to the COPV lay-up geometry, i.e., transverse matrix cracking would be expected to be more important, at least initially, in a COPV with helical and hoop wraps, while is the case of uniaxial strand, fiber breakage predominated throughout the entire loading profile (Figure 9).

Regardless, future FFT waveform analyses will focus on using direct waveform data.

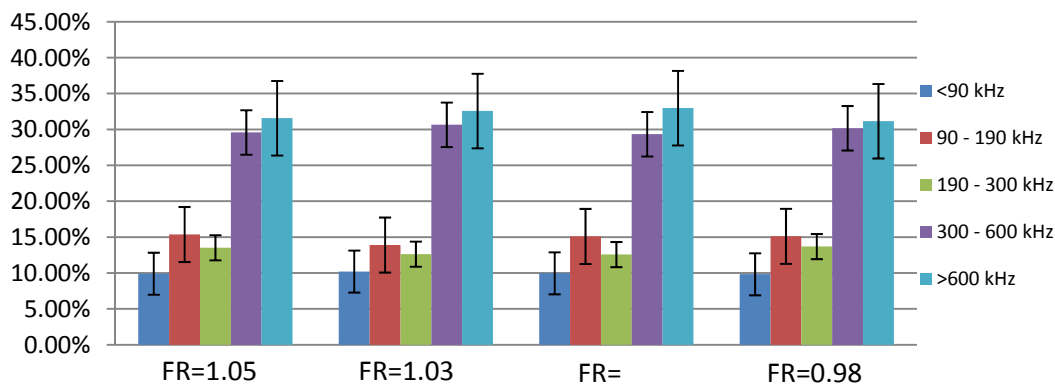


FIGURE 9 Damage distribution for Felicity ratio events of three IM7 carbon-epoxy 12k strand specimens
NOTE: First 15 significant AE events used for each FR/specimen

SUMMARY

FR was found to decrease linearly with increasing stress during ILH testing of T1000 and IM7 composite strand specimens and a IM7 COPV. ILH tests on C/Ep strand showed that FR^* behaves like a universal failure parameter that exhibits less scatter than the tensile strength, or by analogy the burst pressure of a COPV. This suggests that FR^* can be used as an analytical Pass/Fail criterion for C/Ep composite materials and components. For example, data are presented to show FR^* could successfully predict the burst pressure, P^* , of a COPV.

FFT waveform analysis revealed the presence of three primary characteristic waveforms. These were matrix cracking, fiber breakage, and a cooperative failure mode consisting of cracking, breakage, and fiber-matrix debonding and pull-out. Contrary to expectation, low energy events were found to correspond to a predominant fiber breakage mechanism that was independent of LR , while high energy events exhibited a mixture of all forms of micromechanical damage. Inspection of early and late life FFTs revealed that early life events tended to exhibit similar frequency distributions and the observed peaks of comparable amplitude and width, while late life events exhibited a larger range of frequencies, with the observed peaks showing few similarities in peak amplitude and width. It was also demonstrated that FR events are composed primarily of fiber breakage regardless of LR . This suggests that it might be easier and more valid to base accept-reject criteria for C/Ep materials on calculated estimates of accumulated fiber damage at known levels of the FR .

ACKNOWLEDGMENTS

The authors are grateful to Ben Gonzalez and Brooks Wolle (NASA White Sands Test Facility (WSTF)) for help developing the tabbing procedure and help with ILH strand testing, to Ralph Lucero (WSTF) for COPV-level ILH testing, and to Anthony Carden (WSTF) help configuring the DWC AE system. Ongoing efforts at WSTF to develop AE methods specific to carbon-epoxy COPVs have been sponsored by the Office of Safety and Mission Assurance Office, NASA, Washington, DC.

REFERENCES

1. AIAA S-081A-2006, *Space Systems – Composite Overwrapped Pressure Vessels (COPVs)*, American Institute of Aeronautics and Astronautics, Reston, VA (2006).
2. J. Awerbuch and S. Ghafari, "Monitoring Progression of Matrix Splitting During Fatigue Loading Through Acoustic Emission in Notched Unidirectional Graphite/Epoxy Composites," *J. Reinforced Plastics and Composites*, **7**, pp. 245-263 (1988).
3. T. Ely and E. Hill, "Longitudinal Splitting and Fiber Breakage Characterization in Graphite Epoxy Using Acoustic Emission Data," *Matl. Eval.*, 288-294 (1995).
4. P. De Groot, P. Wijnen, and R. Janssen, "Real-time Frequency Determination of Acoustic Emission for Different Fracture Mechanisms in Carbon/Epoxy Composites," *Composites Sci. Technol.*, **55**, pp. 405-421 (1995).
5. W. H. Prosser, K. E. , Jackson, S. Kellas, B. T. Smith, J. McKeon, and A. Friedman, "Advanced, Waveform Based Acoustic Emission Detection of Matrix Cracking in Composites," *Matls. Eval.*, **53**:9, pp. 1052-1058 (1995).

-
6. M. Shiwa, S. Carpenter, and T. Kishi, "Analysis of Acoustic Emission Signals Generated during the Fatigue Testing of GFRP," *J. Composite Matls.*, **30**:18, pp. 2019-2041 (1996).
 7. El Guerjouma, J.-C. Baboux, D. Ducret, N. Godin, P. Guy, S. Huguet, Y. Jayet, and T. Monnier, "Non-Destructive Evaluation of Damage and Failure of Fibre Reinforced Polymer Composites Using Ultrasonic Waves and Acoustic Emission," *Adv. Eng. Matl.*, **3**:8, pp. 601-608 (2001).
 8. S. Huguet, N. Godin, R. Gaertner, L. Salmon, and D. Villard, "Use of Acoustic Emission to Identify Damage Modes in Glass Fibre Reinforced Polyester," *Composites Sci Technol.*, **62**, pp. 1433-1444 (2002).
 9. Y. A. Dzenzis and J. Qian, "Analysis of Microdamage Evolution Histories in Composites," *Int. J. Solids and Structures*, **38**, pp.1831-1854 (2001).
 10. ASTM E 1118, *Standard Practice for Acoustic Emission Examination of Reinforced Thermosetting Resin Pipe (RTRP)*, American Society for Testing and Materials, West Conshohocken, PA (2005).
 11. ASTM E 1067, *Standard Practice for Acoustic Emission Examination of Fiberglass Reinforced Plastic Resin (FRP) Tanks/Vessels*, American Society for Testing and Materials, West Conshohocken, PA (2007).
 12. ASTM E 976, *Guide for Determining the Reproducibility of Acoustic Emission Sensor Response*, American Society for Testing and Materials, West Conshohocken, PA (2005).
 13. J. M. Waller, R. L. Saulsberry, and E. Andrade, "Use of Acoustic Emission to Monitor Progressive Damage Accumulation in Kevlar® 49 Composites," *QNDE Conference*, Providence, RI, July 2009.
 14. Nichols, C. T., Waller, J. M., and Saulsberry, R. L., "Use of Acoustic Emission to Monitor Progressive Damage Accumulation in Carbon Composites," *USRP Final Report*, NASA-JSC Whites Sands Test Facility, Las Cruces, NM, December 2009.
 15. D. J., Wentzel, J. M. Waller, R. L. Saulsberry, "Progression of Micromechanical Damage in Carbon Fiber/Epoxy Tows," *USRP Final Report*, Las Cruces, NM, May 2010.
 16. C. T. Nichols, J. M. Waller, R. L. Saulsberry, R. L., "Acoustic Emission Lifetime Estimation for Carbon Fiber/Epoxy Composite Overwrapped Pressure Vessels," *USRP Final Report*, NASA-JSC Whites Sands Test Facility, Las Cruces, NM, August 2010.
 17. L. Grimes-Ledesma, S. L., Phoenix, H. Beeson, T. Yoder, and N. Greene, "Testing of Carbon Fiber Composite Overwrapped Pressure Vessel," NASA-Jet Propulsion Laboratory, Pasadena, CA, 2006.
 18. M. A. Hamstad, University of Denver, private communication, January 2010.
 19. K. S. Downs and M.A. Hamstad "Acoustic Emission from Depressurization to Detect/Evaluate Significance of Impact Damage to Graphite/Epoxy Pressure Vessels," *J. Composite Matls.*, Vol. 32, No. 3, 1998, pp. 258-307.